

# Comparative study of multi-functional luminogens with 1,3,5-triazine as the core and phenothiazine or phenoxy donors as the peripheral moieties for non-doped/doped fluorescent and red phosphorescent OLEDs

Xiao-Feng Tan<sup>a,b,1</sup>, Pei-Pei Wang<sup>a,1</sup>, Ling Lu<sup>a</sup>, Oleksandr Bezikonnyi<sup>b,c</sup>, Dmytro Volyniuk<sup>b</sup>, Juozas Vidas Grazulevicius<sup>b,\*</sup>, Qing-Hua Zhao<sup>a,\*\*</sup>

<sup>a</sup> College of Materials Science and Engineering, Huaqiao University, Xiamen, 361020, China

<sup>b</sup> Department of Polymer Chemistry and Technology, Kaunas University of Technology, K. Baršausko g. 59, Kaunas, Lithuania

<sup>c</sup> Experimental Physics Department, Faculty of Physics, Taras Shevchenko National University of Kyiv, pros. Akademika Glushkova 4b, Kyiv, Ukraine

## ABSTRACT

A series of three-armed fluorescent emitters based on a 1,3,5-triazine acceptor as the central core and phenothiazine or phenoxy moieties as the different peripheral units, are designed and synthesized. All of them exhibit aggregation-induced emission enhancement and thermally activated delayed fluorescence. Photoluminescence quantum yields exceeded 37 and 67% for non-doped and doped solid-state samples respectively. The compounds were found to be capable of transporting both holes and electrons. The highest mobility values of more than  $1 \times 10^{-4} \text{ cm}^2 \text{ V}^{-1} \text{ s}^{-1}$  were obtained for the compound having three phenothiazine moieties at electric field of more than  $1 \times 10^6 \text{ V cm}^{-1}$ . Additionally, three types of organic light emitting diodes based on these materials were fabricated. The device containing non-doped emission layer with the compound containing single phenothiazine moiety as the emitter gave maximum external quantum efficiency of 5.4%. The device with doped emission layer containing 5% solid solution of the compound having three phenothiazine moieties in an appropriate host gave maximum external quantum efficiency of 9.9%. The phosphorescent device hosted by the compound with single phenothiazine unit exhibited maximum external quantum efficiency of 10.3% and a low-efficiency roll-offs of 1% at  $1000 \text{ cd/m}^2$ .

## 1. Introduction

Thermally activated delayed fluorescence (TADF) has attracted significant attention because of easily activated reverse intersystem crossing (RISC) by the thermal motion of atoms [1]. The real breakthrough of harvesting both singlet and triplet excitons, as well as an internal quantum efficiency (IQE) of 100% for organic light emitting diodes (OLEDs), was achieved by Adachi et al., in 2011 [2]. An ideal TADF material needs to have at least two important features: (i) a large RISC rate constant ( $k_{\text{risc}}$ ) for better utilization of non-emissive triplet excitons; (ii) a relatively large radiative rate constant ( $k_r$ ) for achieving high electroluminescence (EL) efficiency [3]. However, the large  $k_{\text{risc}}$  and  $k_r$  sometimes are conflicting, which make the design of TADF molecules knotty and difficult. Numerous theoretical researches disclosed that  $k_{\text{risc}}$  is inversely proportional to the energy gap ( $\Delta E_{\text{ST}}$ ) between singlet excited state ( $S_1$ ) and triplet excited state ( $T_1$ ) [4]. The interaction of electron-donating and electron-accepting moieties resulting in intramolecular charge transfer leads to small  $\Delta E_{\text{ST}}$  by spatially separating highest occupied molecular orbital (HOMO) and lowest

unoccupied molecular orbital (LUMO) of molecules [5]. In most cases, donor-acceptor systems or conjugation-breaking molecular structures are used to obtain small  $\Delta E_{\text{ST}}$  for TADF emitters [6]. As for  $k_r$ , it is related to the overlapping density ( $\rho_{10}$ ) between the electronic wave functions of the ground state ( $S_0$ ) and the lowest excited singlet state ( $S_1$ ) [7]. Usage of phenyl linkage or multiple donor/acceptor systems can increase the overlapping density and allow to achieve high EL efficiency [8]. Specifically, extending the molecular orbitals while limiting the overlap between HOMO and LUMO can suppress a decrease in  $k_r$  while lowering  $\Delta E_{\text{ST}}$  [6].

Most of the pure organic TADF molecules are of donor-acceptor (D-A) type with the twisted structures or big steric hindrance between the donor and acceptor units [9], such as derivatives of triazine [10,11], thioxanthone [12], oxadiazole [13] and sulfones [14]. In general, most of the discovered TADF molecules require to be doped into some rigid host materials with high triplet energy levels [15]. However, majority of TADF materials commonly suffer from aggregation-caused quenching in the condensed state, which makes EL device structures more complicated due to the requirement of doping of

\* Corresponding author.

\*\* Corresponding author.

E-mail address: [juozas.grazulevicius@ktu.lt](mailto:juozas.grazulevicius@ktu.lt) (J.V. Grazulevicius).

<sup>1</sup> Xiaofeng Tan and Peipei Wang share the same contribution for this article.

emitter molecules in some properly selected host materials [16]. In 2001, Tang et al. [17,18] demonstrated the mechanism of aggregation-induced emission (AIE) in which light emission can be dramatically enhanced in the condensed phase. After that, numerous AIE luminophores have attracted extensive attention for their potential application in OLEDs [19,20] and fluorescent molecular sensors [21,22]. Therefore, it is of great interest to obtain enhanced light emission in the condensed phase and generate efficient OLEDs with simple non-doped device structures, if TADF materials also possess AIEE ability. Based on the design concept, several groups have reported the successful cases of the combination of prominent TADF and AIEE properties [23]. Recently, Tang et al. [24] synthesized a new tailor-made material DCPDAPM based on carbazole as the skeleton, with 9,9-dimethyl-9,10-dihydroacridine as the donor group and benzophenone as the acceptor group. The non-doped device with the material gave a maximum external quantum efficiency (EQE) of 8.15%, and doped device with DCPDAPM doped into CBP exhibited a maximum EQE of 19.67%. Among the reported AIEE-TADF materials, only a few linear or two-dimensional molecule structures have been investigated [23]. Thus, the development of new AIEE-TADF materials with different types of structures is of great interest.

In this work, a series of three-armed AIEE-TADF materials based on a 1,3,5-triazine acceptor as the core and a phenothiazine donor or a phenoxy donor as the different peripheral units, were developed for use in OLEDs. Triazine (TRZ) was widely used as the electron-withdrawing moiety of D-A materials because of its high electronic deficiency and three scattered modifiable positions [25]. Phenothiazine moiety linked the triazine core via phenyl bridge or phenoxy group linked the triazine core via oxygen atom were selected as the different peripheral units to constitute AIEE-TADF materials. The effect of the different peripheral units on the properties of obtained materials were explored in detail. Compared with the common carbazole donor, phenothiazine moiety brings more steric repulsion because of its morpholine-like six-membered ring and can better localize the electron density distribution of the HOMO onto the donor unit [26]. Additionally, phenoxy unit is also beneficial for realizing the TADF character for the materials, as it was previously reported [27].

## 2. Results and discussions

### 2.1. Synthesis

Synthesis of PTZ-TROZ, bis-PTZ-TROZ, and tri-PTZ-TROZ is shown in Scheme 1. 1,3,5-triazine-based compounds can be easily synthesized by Suzuki coupling reaction. The detailed synthesis procedures are given in the experimental section. The target compounds were characterized by  $^1\text{H}$  and  $^{13}\text{C}$  NMR, and high-resolution mass spectrometry.

### 2.2. Thermal characterization

Thermogravimetric analysis (TGA) and differential scanning calorimetry (DSC) measurements in a wide range of temperature were performed for the samples of PTZ-TROZ, bis-PTZ-TROZ, and tri-PTZ-TROZ. The results are collected in Fig. 1 and Table 1. With the increasing number of PTZ units, 5% weight loss temperatures of the compounds increased in the range of 328 °C, 365 °C, 421 °C (Fig. 1a). Similarly, DSC curves showed the increase of glass transition temperatures in the range of 75 °C, 95 °C, 114 °C (Fig. 1b). The thermal stability of PTZ-TROZ, bis-PTZ-TROZ, and tri-PTZ-TROZ gradually improved due to the increase of rigid phenothiazine units.

### 2.3. Theoretical studies

Natural transition orbitals (Fig. 2a) and hole/electron distribution (Fig. 2b) for the S1 state of the compounds were depicted by Multiwfn (a multifunctional wavefunction analyzer) to study the hole and

electron distribution [28]. It is obvious that the S1 states of all three compounds are pure CT states and the transition can be well represented by a pair of natural transition orbitals. However, since holes and electrons are almost entirely localized on phenothiazine and triazine units, the transition from hole to electron is hard to be noticed, because the oscillator strength is close to zero. In order to analyze the quantitative characterization of hole and electron distribution differences, two parameters were introduced.  $S_r$  index was used to characterize the overlapping extent of hole and electron, while  $t$  index was designed to measure separation degree of hole and electron in CT direction. The two parameters are written as:

$$S_r \text{ index} = \int S_r(r) dr \equiv \int \sqrt{\rho^{\text{hole}}(r)\rho^{\text{ele}}(r)} dr$$

$$t \text{ index} = D \text{ index} - H_{\text{CT}}$$

where  $\rho^{\text{hole}}$  and  $\rho^{\text{ele}}$  refer to the density of hole and electron,  $D$  index refers to the total magnitude of CT length,  $H_{\text{CT}}$  refers to the average degree of spatial extension of hole and electron distribution in CT direction [28,29]. PTZ-TROZ showed the largest  $S_r$  index, which means that PTZ-TROZ has the best overlapping of hole and electron. Bis-PTZ-TROZ showed the largest  $t$  index which implies that bis-PTZ-TROZ has the best separation of holes and electrons which was allowed to predict smaller  $\Delta E_{\text{ST}}$  [30,31].

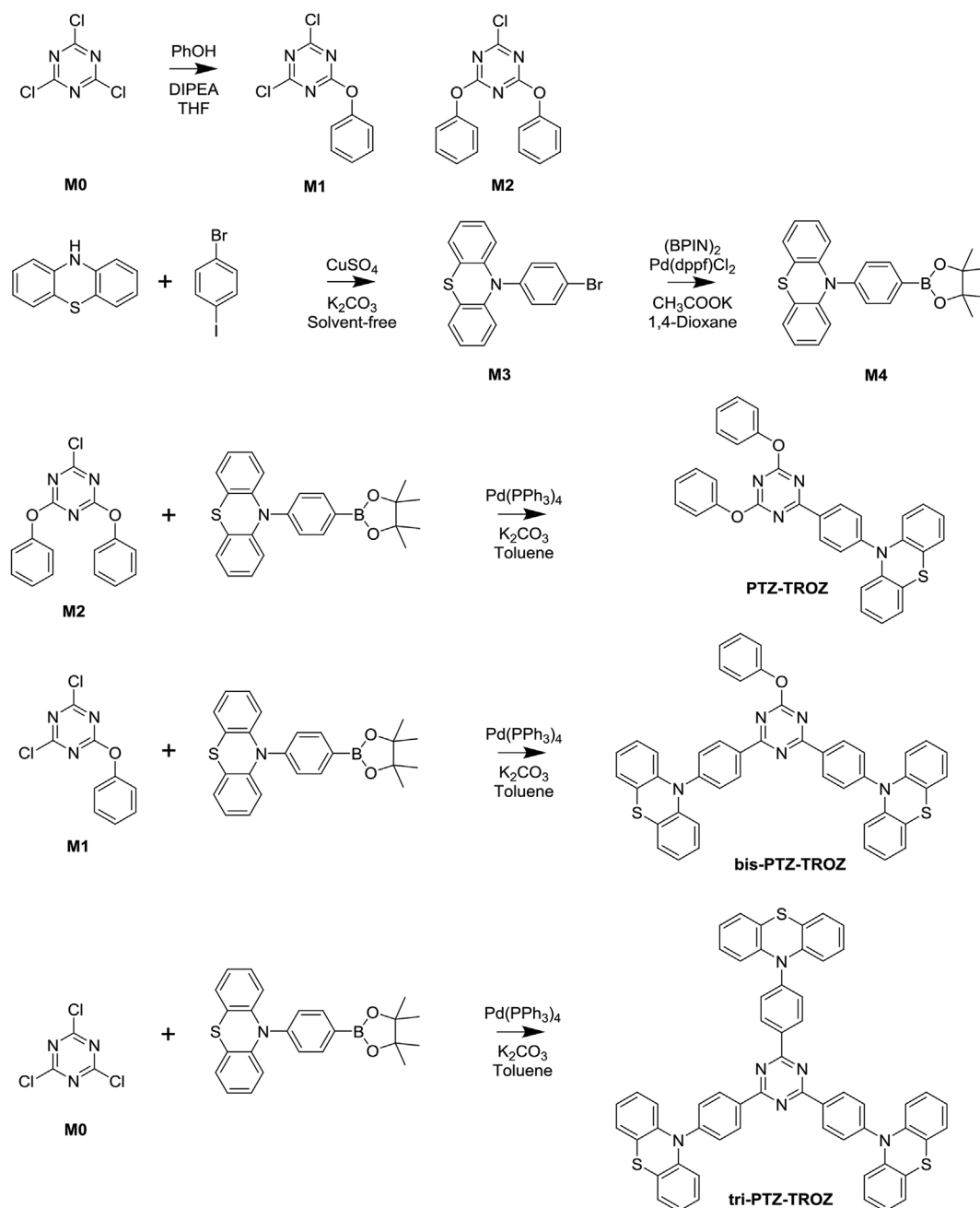
### 2.4. Electrochemical properties

HOMO and LUMO of the molecules can be estimated by measuring ionization potentials (IP) and electron affinities (EA) by cyclic voltammetry (CV), since they have same absolute values. CV curves of PTZ-TROZ, bis-PTZ-TROZ, and tri-PTZ-TROZ (Fig. 3) exhibited an oxidation peak with the onset oxidation potential ( $E_{\text{ox}}$ ) at 0.75 eV, 0.73 eV, 0.68 eV (Table 1). The values of IP were calculated to be 5.55 eV, 5.53 eV, 5.48 eV, respectively from the empirical formula  $E_{\text{IP}} = E_{\text{ox}} + 4.8$  eV. The energies of EA were obtained to be 2.71 eV, 2.68 eV, 2.61 eV, respectively from the empirical formula  $E_{\text{EA}} = E_{\text{IP}} - E_{\text{opt}}$ , where  $E_{\text{opt}}$  is an estimate of the energy of the first singlet excited state measured from the onset position of their absorption spectra from Fig. 4a.

### 2.5. Photophysical properties

UV-vis absorption and photoluminescence (PL) spectra of toluene solutions and vacuum deposited films of the studied compounds are plotted in Fig. 4a and S1. Summary of the main photophysical properties of PTZ-TROZ, bis-PTZ-TROZ, and tri-PTZ-TROZ are presented in Tables 2 and 3. All three compounds show  $\pi$ - $\pi^*$  transition absorption band with the maximum at 256 nm and ICT absorption bands at 354, 368 and 370 nm for PTZ-TROZ, bis-PTZ-TROZ, and tri-PTZ-TROZ respectively. The red-shift of ICT absorption bands with the increasing number of PTZ donor units can prove that the ICT was stabilized and delocalized over the PTZ donor units and TRZ core unit. With the increase of solvent polarity, significant red shifts of the emission peaks occurred (Fig. S2), which indicate that the emission originated from the intramolecular charge transfer state. In PL spectra of the films, the fluorescence intensity maxima wavelengths are red-shift with the increase of the number of PTZ donor units from 551 nm for PTZ-TROZ to 557 nm for bis-PTZ-TROZ and 563 nm for tri-PTZ-TROZ. The enhancement of the donor property by increasing number of PTZ donor units induced the delocalization of the ICT state over the D-A molecules. Such stabilization of the ICT states leads to a red-shift of ICT emission. The half-widths of emission bands of the films and solutions showed no big difference. This observation is apparently the result of two factors competing with each other: (i) strengthening of ICT caused by the increasing number of PTZ donor units and (ii) weakening of vibrational motion caused by the decreasing number of phenoxy units.

Dilute toluene solutions of compounds PTZ-TROZ, bis-PTZ-TROZ,



**Scheme 1.** Synthesis of PTZ-TROZ, bis-PTZ-TROZ, and tri-PTZ-TROZ.

and tri-PTZ-TROZ exhibited yellow emission under UV excitation (Fig. S1). Slight red-shifts of the PL spectra of the solutions were observed with the increasing number of PTZ substituents (Table 2). PL spectra of the vacuum-deposited films of PTZ-TROZ, bis-PTZ-TROZ, and tri-PTZ-TROZ exhibited significant red shifts in comparison to PL spectra of the toluene solutions apparently due to the higher polarity of the studied compounds in solid state comparing to that of toluene ( $\epsilon = 2.38$ ) (Fig. 4a, Table 2). Such red-shifts are usual for donor-acceptor compounds exhibiting intramolecular charge transfer (ICT) character of emissions [32].

The deoxygenated solution of PTZ-TROZ, bis-PTZ-TROZ, and tri-PTZ-TROZ in toluene demonstrated low PLQY values of 4.3, 2.4, and 6.4%, respectively. Small differences of PLQY values of PTZ-TROZ, bis-PTZ-TROZ, and tri-PTZ-TROZ can be explained by the differences in their dipole moments induced by the different number of PTZ substituents. Much higher PLQY values of 37, 24, and 15% were recorded

for vacuum-deposited films of PTZ-TROZ, bis-PTZ-TROZ, and tri-PTZ-TROZ, respectively (Table 2). The considerable increase in the emission intensity of the solid state compared to the solution, is usually related to AIEE phenomenon [33]. The additional evidence indicating that the emission of PTZ-TROZ, bis-PTZ-TROZ and tri-PTZ-TROZ compounds in solid state is related to AIEE will be provided in the following sections. It is worth noting that for the doped layers of PTZ-TROZ, bis-PTZ-TROZ, and tri-PTZ-TROZ using mCP as the host, approximately twice higher PLQY values were obtained. This observation can be explained by the enhancement of TADF efficiency of compounds in the host compared with that in non-doped layers, due to the possible changes in dihedral angles between donor and acceptor moieties of PTZ-TROZ, bis-PTZ-TROZ, and tri-PTZ-TROZ. Similar hosting effects on TADF emitters were studied elsewhere [34]. In addition, mCP host, which molecular structure is not appropriate for the hydrogen bonding, may restricts intermolecular interactions (such as the  $\pi$ - $\pi$  stacking or hydrogen bonds

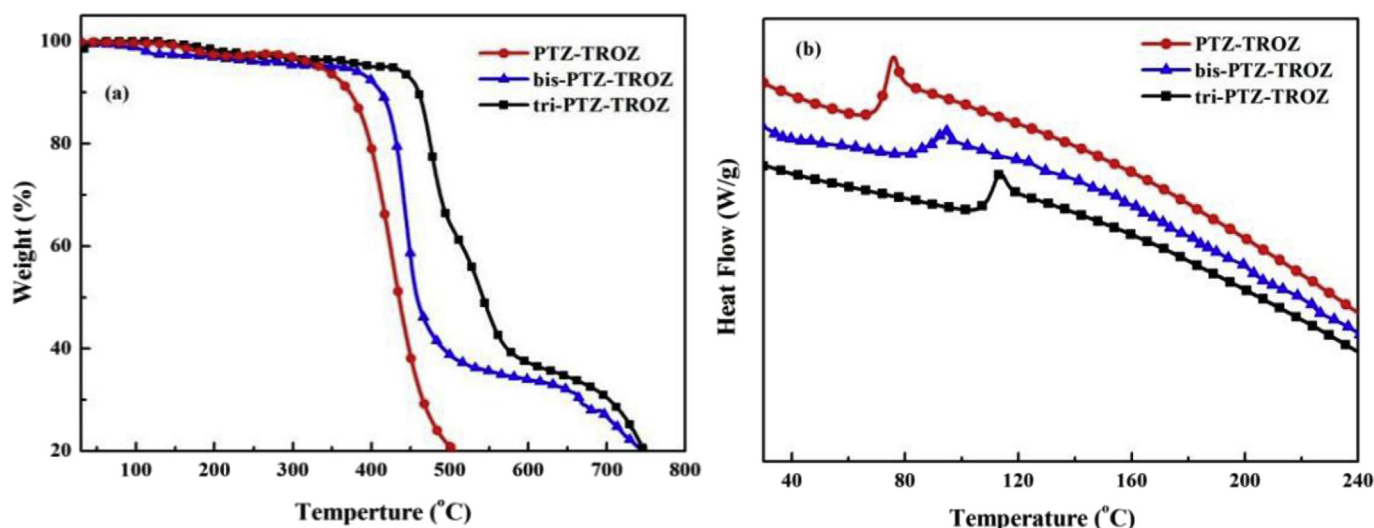


Fig. 1. TGA (a) and DSC (b) curves of PTZ-TROZ, bis-PTZ-TROZ, and tri-PTZ-TROZ.

[35]) between neighboring molecules in solid state of PTZ-TROZ, bis-PTZ-TROZ, and tri-PTZ-TROZ, which molecular structures are well appropriate for the hydrogen bonding since they includes oxygen and sulfur atoms. As a result, higher PLQY values of 64, 67 and 63% for the doped films mCP:PTZ-TROZ, mCP:bis-PTZ-TROZ, and mCP:tri-PTZ-TROZ were obtained in comparison to PLQY values for the non-doped films PTZ-TROZ, bis-PTZ-TROZ, and tri-PTZ-TROZ, respectively (Table 2). PLQYs of 28, 33 and 37% for the films of molecular mixtures DPEPO:PTZ-TROZ, DPEPO:bis-PTZ-TROZ, and DPEPO:tri-PTZ-TROZ, respectively, were additionally measured using bis[2-(diphenylphosphino)phenyl] ether oxide (DPEPO) as a host molecular structure of which is favourable for hydrogen bonding. This result partly supports above described assumption that the restriction of intermolecular interactions can cause PLQY enhancement even for AIEE emitters.

PL spectroscopy measurements were performed for degassed and non-degassed solutions of the compounds (Fig. 4b and c). PL decay curves with typical TADF material characteristics were obtained for the studied compounds PTZ-TROZ, bis-PTZ-TROZ and tri-PTZ-TROZ (Fig. 4c). In addition, for the deoxygenated toluene solution and films, an increase in the intensity of the long-lived emission component was detected, indicating the contribution of the triplet excitons (Fig. 4c and S8). Fig. 4b and c shows that, with the increasing number of PTZ substituents, the contribution of delayed fluorescence in the fluorescence spectra increased. This observation may be explained by the large delocalization of molecular orbitals in the structures with well-separated HOMO and LUMO and by increased dipole moment of transition between S0 and S1. To explain the increasing intensity of the long-lived emission components, we consider that the increase of PTZ units stabilized the ICT state.

To evaluate the singlet-triplet splitting for the tested compounds, PL and phosphorescence spectra of the solutions in THF were recorded at 77 K (Fig. 4d). From the difference between the onsets of fluorescence and phosphorescence spectra,  $\Delta E_{ST}$  was determined to be 0.42 eV, 0.38 eV, and 0.43 eV for PTZ-TROZ, bis-PTZ-TROZ, and tri-PTZ-TROZ,

respectively (Table 2). Taking into account the relatively large  $\Delta E_{ST}$  values, inefficient TADF is expected for the solutions of PTZ-TROZ, bis-PTZ-TROZ, and tri-PTZ-TROZ confirmed by small PLQY values (Table 2). With the increase of the number of PTZ units and with the decrease of the number of phenoxy units in the studied molecules, their triplet state energy values decreased gradually.

Due to the similarity of fluorescence and phosphorescence spectra, practically identical PL spectra were recorded for the films of the compounds at different temperatures (Fig. 5a and S3). In contrast to the relatively high  $\Delta E_{ST}$  values observed for the THF solutions, small  $\Delta E_{ST}$  values of 0.07, 0.02, and 0.07 eV were recorded for the solid films of PTZ-TROZ, bis-PTZ-TROZ, and tri-PTZ-TROZ, which promoted the generation of TADF (Fig. 5b, Table 2). Therefore, PLQYs of the undoped films were found to be considerably higher than those of the solutions. PL decay curves recorded at different temperatures indicate that intensity of the long-lived emission component increases with the decreasing temperature. This observation confirms the TADF character of delayed fluorescence (Fig. 5c and S3).

To analyze the relative contribution of prompt and delayed components to the whole relaxation processes, we fitted PL decays of deoxygenated toluene solutions and of the films of molecular mixtures PTZ-TROZ:mCP, bis-PTZ-TROZ:mCP, tri-PTZ-TROZ:mCP (Fig. 4b and S7b). By fitting the formula shown below, the radiation transition rates of the doped films of the compounds were calculated [36].

$$k_{PF} = \frac{\eta_{PF}}{\tau_{PF}} \quad k_{ISC} = \frac{\eta_{DF}}{\eta_{PF} + \eta_{DF}} k_{PF}$$

$$k_{DF} = \frac{\eta_{DF}}{\tau_{DF}} \quad k_{RISC} = \frac{\eta_{DF} \cdot k_{PF} \cdot k_{DF}}{\eta_{PF} \cdot k_{ISC}}$$

where  $k_{PF}$ ,  $k_{DF}$ ,  $k_{ISC}$ , and  $k_{RISC}$  are rate constants of prompt and delayed components, intersystem crossing (ISC) and RISC processes, respectively;  $\eta_{PF}$  and  $\eta_{DF}$  are prompt and delayed PLQYs which can be distinguished from the total PLQY by comparing the integrated intensity of the prompt and delayed components in the transient photoluminescence spectra (Table 3).

Table 1

Energies of frontier molecular orbitals and ground/excited states of PTZ-TROZ, bis-PTZ-TROZ, and tri-PTZ-TROZ.

Sample	T <sub>d</sub> (°C)	T <sub>g</sub> (°C)	E <sub>opt</sub> <sup>b</sup> (eV)	E <sub>ox</sub> (eV)	HOMO <sup>a</sup> (eV)	LUMO <sup>a</sup> (eV)
PTZ-TROZ	328	75	2.84	0.75	-5.55	-2.71
bis-PTZ-TROZ	365	95	2.85	0.73	-5.53	-2.68
tri-PTZ-TROZ	421	114	2.87	0.71	-5.48	-2.61

<sup>a</sup> Calculated from the empirical formula E<sub>HOMO</sub> = -(E<sub>ox</sub> + 4.8), E<sub>LUMO</sub> = E<sub>HOMO</sub> - E<sub>opt</sub>.

<sup>b</sup> Estimated from the onset of the absorption edge of the thin films.

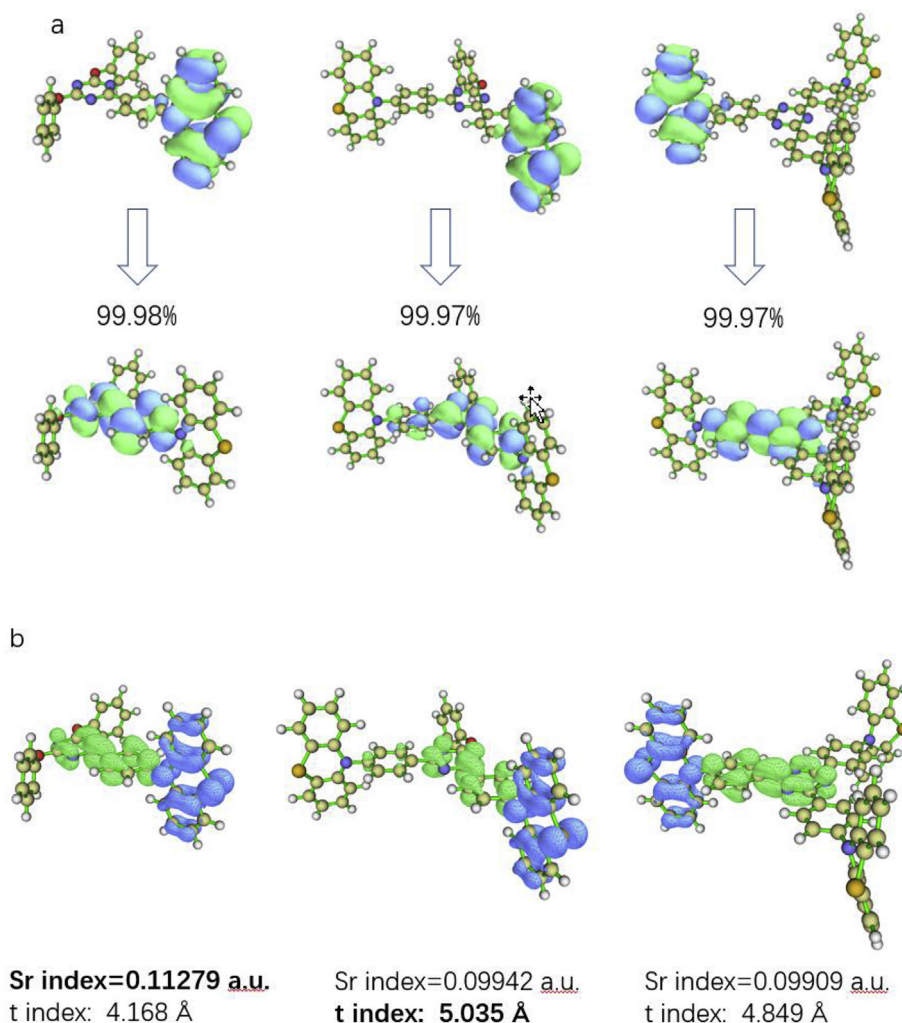


**Fig. 2.** Natural transition orbital (a) and hole/electron distribution (b) of PTZ-TROZ, bis-PTZ-TROZ, and tri-PTZ-TROZ.

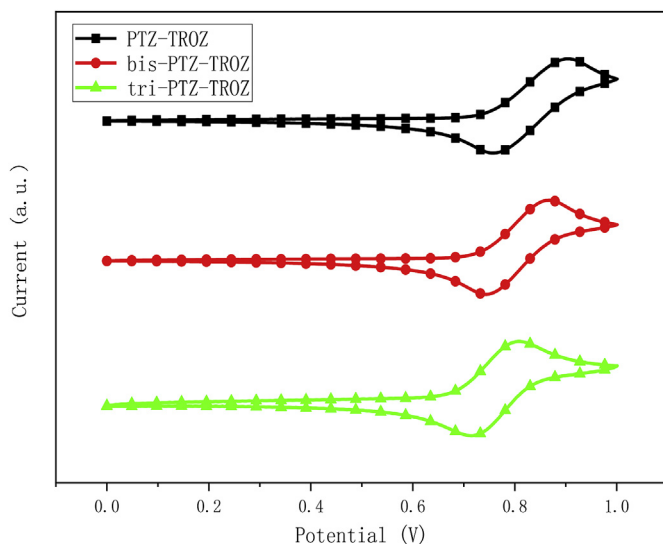


**Fig. 3.** CV curves of PTZ-TROZ, bis-PTZ-TROZ, and tri-PTZ-TROZ.

Because of smaller  $\Delta E_{ST}$  values of the solid samples of the compounds than those of the solutions (Table 2), higher  $k_{DF}$  and  $k_{RISC}$  by one order of magnitude were obtained for the films of PTZ-TROZ:mCP, bis-PTZ-TROZ:mCP, and tri-PTZ-TROZ:mCP. For this reason, the doped

films exhibited higher TADF efficiency than the solutions (Table 3). The studied compounds in solid state exhibited relatively high  $k_{RISC}$  values which are comparable with those of highly efficient TADF emitters [37].

## 2.6. Aggregation induced emission enhancement

PL spectra of the dispersions of the compounds in the THF: water systems were recorded for estimation of their AIEE properties [38]. The most representative experiment to prove AIE characteristics. PTZ-TROZ, bis-PTZ-TROZ, and tri-PTZ-TROZ showed good solubility in THF, but they were insoluble in water (Fig. 6 and S4). In contrast to very weak emission of THF solutions of the compounds, dispersions of PTZ-TROZ, bis-PTZ-TROZ, and tri-PTZ-TROZ in THF and water mixtures exhibited strong emission after formation of aggregates in the mixtures with high water fraction (> 80%). The AIEE effect was observed for the compounds due to the restriction of rotations and vibrations of PTZ and phenoxy units relative to triazine moieties in solid aggregates. When the molecules are in solution, the peripheral phenothiazine and phenoxy can be freely rotated by a single bond around the center of the 1,3,5-triazine [39]. This process consumes the excited state energy in a non-radiative transition, resulting in weak fluorescence. However, in the aggregate state, the “propeller” configuration of the molecule can prevent the  $\pi$ - $\pi$  stacking and inhibit the fluorescence quenching. At the same time, due to the space constraints, the intramolecular rotation limitation inhibits the non-radiative transition

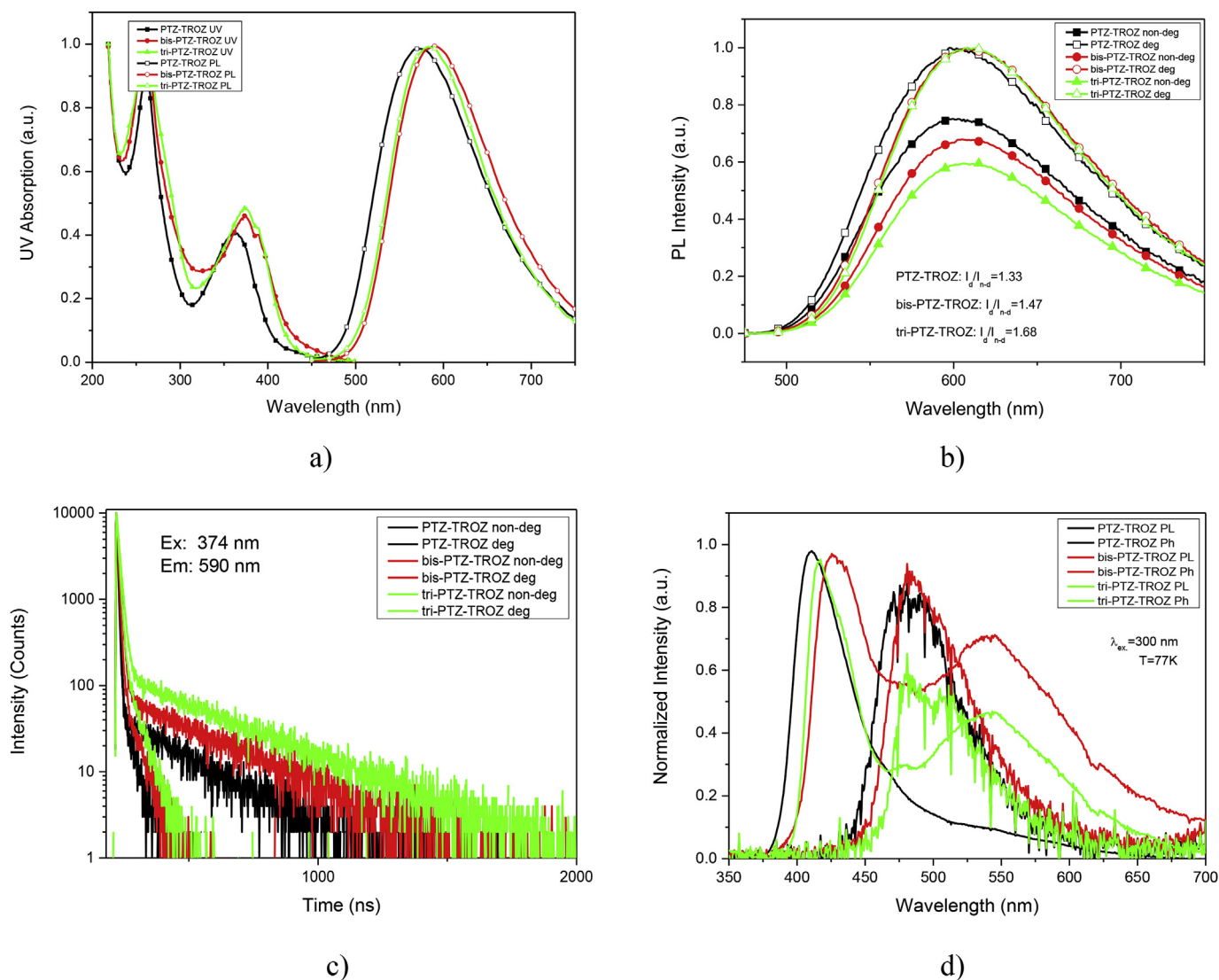


**Fig. 4.** UV and PL spectra of vacuum deposited films of PTZ-TROZ, bis-PTZ-TROZ, and tri-PTZ-TROZ (a); PL spectra (b) and emission decay curves (c) of the degassed and non-degassed solutions in toluene at room temperature; and PL and phosphorescence spectra (d) of the solutions in THF recorded at 77 K. Excitation wavelengths have to be given for PL spectra.

channel of the excited state, opens the radiation transition channel, thereby enhancing fluorescence [40,41].

## 2.7. Charge-injecting and charge-transporting properties

With the purpose to unclose the potential of PTZ-TROZ, bis-PTZ-TROZ, and tri-PTZ-TROZ for optoelectronic application, charge-injecting and charge-transporting properties of their solid samples were investigated. The key parameters of organic electroactive materials, i.e., ionization potentials ( $I_p^{EP}$ ), electron affinities ( $E_A^{PE}$ ) and charge-drift

mobilities ( $\mu$ ) were determined by photoelectron emission spectroscopy and time-of-flight (ToF) measurements, respectively. By extrapolation of liner part of photoelectron emission spectra of vacuum-deposited films of PTZ-TROZ, bis-PTZ-TROZ, and tri-PTZ-TROZ to abscissa axis (Fig. 7), practically identical  $I_p^{EP}$  values of ca. 5.4 eV were obtained for the compounds. This observation shows that they are appropriate for efficient hole-injection from the common ITO anode of the optoelectronic devices. Using optical band gaps  $E_g$ , close  $E_A^{PE}$  values of ca. 2.57 eV were obtained for the samples of PTZ-TROZ, bis-PTZ-TROZ, and tri-PTZ-TROZ by the equation  $E_A = I_p^{PE} - E_g$ . These values enable to

**Table 2**  
Summary of photophysical properties of PTZ-TROZ, bis-PTZ-TROZ, and tri-PTZ-TROZ.

Sample	$\lambda_{max,abs}$ (nm)	$\lambda_{max,PL}$ (nm)	$S1^a$ (eV)	$T1^a$ (eV)	$\Delta E_{ST}$ (eV)	PLQY (%)
	Toluene/neat film			THF/neat film		Toluene/neat film/mCP doped film
PTZ-TROZ	256, 355/261, 363	549/585	3.21/2.59	2.79/2.53	0.42/0.07	4.9/37/64
bis-PTZ-TROZ	255, 364/260, 374	558/596	3.12/2.49	2.74/2.47	0.38/0.02	2.4/24/67
tri-PTZ-TROZ	256, 365/262, 374	562/591	3.11/2.57	2.68/2.5	0.43/0.07	6.4/15/63

<sup>a</sup> To calculate the singlet (S1) and triplet (T1) energy levels of the studied compounds, empiric formula  $E_S = 1239/\lambda_S$ , and  $E_T = 1239/\lambda_T$  was used, where  $\lambda_S$  and  $\lambda_T$  are wavelengths of onsets of fluorescence and phosphorescence spectra (Fig. 4a).

**Table 3**  
Rate constants of prompt and delayed components of the deoxygenated toluene solutions and doped films of PTZ-TROZ, bis-PTZTROZ, and tri-PTZ-TROZ.

Compound	$\tau_{PF}$ , ns	$\tau_{DF}$ , $\mu$ s	$\eta_{PF}$	$\eta_{DF}$	$k_{PF}$ , $s^{-1}$	$k_{ISC}$ , $s^{-1}$	$k_{DF}$ , $s^{-1}$	$k_{RISC}$ , $s^{-1}$
In toluene								
PTZ-TROZ,	8.75 (78%)	0.3 (22%)	0.038	0.011	$7.8 \times 10^6$	$1.75 \times 10^6$	$0.4 \times 10^5$	$0.52 \times 10^5$
bis-PTZ-TROZ	5.13 (83%)	0.26 (17%)	0.02	0.004	$8.3 \times 10^6$	$1.38 \times 10^6$	$0.15 \times 10^5$	$0.18 \times 10^5$
tri-PTZ-TROZ	12 (72%)	0.36 (28%)	0.046	0.018	$7.2 \times 10^6$	$2 \times 10^6$	$0.5 \times 10^5$	$0.7 \times 10^5$
In mCP								
PTZ-TROZ,	11 (34%)	1.1 (66%)	0.22	0.44	$2 \times 10^7$	$1.4 \times 10^7$	$4 \times 10^5$	$1.14 \times 10^6$
bis-PTZ-TROZ	7.3 (69%)	0.8 (31%)	0.46	0.21	$6.3 \times 10^7$	$2 \times 10^7$	$2.6 \times 10^5$	$0.29 \times 10^6$
tri-PTZ-TROZ	8 (33%)	1 (67%)	0.21	0.42	$2.6 \times 10^7$	$1.73 \times 10^7$	$4.2 \times 10^5$	$1.26 \times 10^6$

predict efficient electron injection from the common LiF/Al cathode. These energy levels are in excellent agreement with the data of CV measurements described in the previous section. The increase in the number of PTZ units practically leads to tiny shifts of HOMO and LUMO values.

To study the impact of the number of donor substituents on charge carrier transport in the vacuum-deposited layers of the compounds, ToF measurements we performed [42]. Depending on the polarity of applied voltages, holes or electrons were generated in the vacuum-deposited

layers of PTZ-TROZ, bis-PTZ-TROZ, and tri-PTZ-TROZ by light excitation through the ITO electrode using a pulsed laser ( $\lambda = 355$  nm). Under different external electric fields, the photogenerated either holes or electrons were transported through the layer from the ITO electrode to the opposite Al electrode. The transit times ( $t_{tr}$ ) were well-observed for charges in the corresponding low-dispersive photocurrent transients of the tested samples (Fig. 7a and S5). Taking  $t_{tr}$  from photocurrent plots in log-log scale as it was described earlier [43], hole ( $\mu_h$ ) and electron ( $\mu_e$ ) mobilities were calculated and presented in Fig. 7b

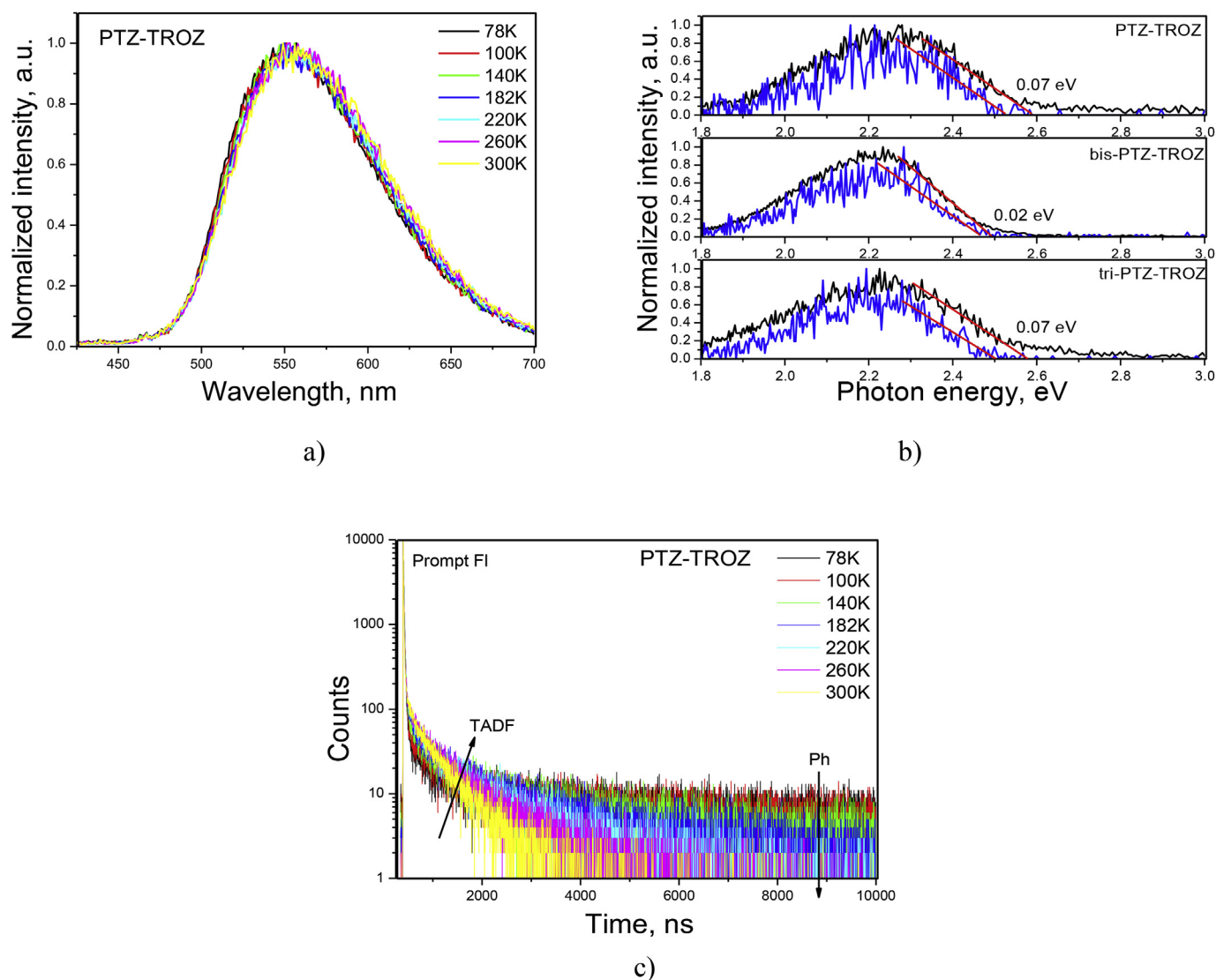


**Fig. 5.** PL and phosphorescence spectra (a) of the solid films of PTZ-TROZ, bis-PTZ-TROZ, and tri-PTZ-TROZ recorded at 77 K; PL spectra (b) and PL decay curves (c) of the solid film of PTZ-TROZ recorded at different temperatures.

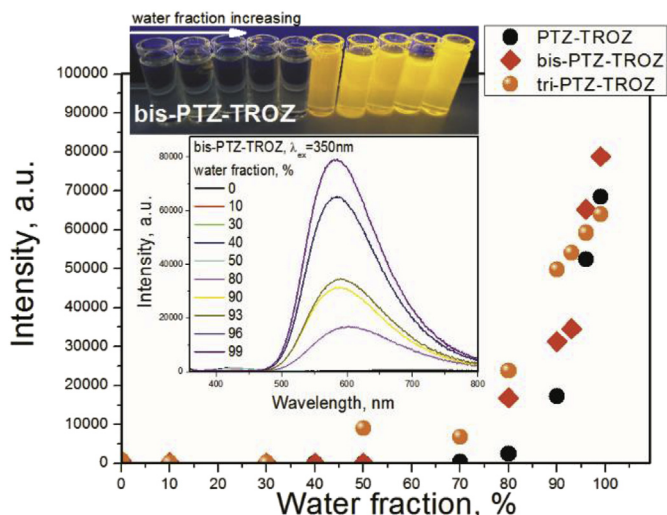


Fig. 6. PL intensity versus water fraction in THF: water mixtures. Insets: PL spectra and photos under UV excitation of bis-PTZ-TROZ dispersed in THF: water mixtures with the different water content.

according to the Poole–Frenkel mobility-electric field (E) relationship  $\mu = \alpha_0 e^{\alpha E^{1/2}}$ , where  $\alpha$  is the field dependence parameter [44]. PTZ-TROZ containing single PTZ unit was characterized by  $\mu_h$  of  $3.2 \times 10^{-6} \text{ cm}^2 \text{V}^{-1} \text{s}^{-1}$  and  $\mu_e$  of  $3.3 \times 10^{-5} \text{ cm}^2 \text{V}^{-1} \text{s}^{-1}$  at an electric field of  $9.4 \times 10^5 \text{ Vcm}^{-1}$ . Thus PTZ-TROZ exhibited by ca. one order of magnitude lower hole mobility in comparison to its electron mobility. In contrast, bis-PTZ-TROZ and tri-PTZ-TROZ showed close values of hole and electron mobilities indicating well-balanced charge transport over a large range of electric fields (Fig. 7b). The similar electron mobility values of  $1.1 \times 10^{-5}$ ,  $2.2 \times 10^{-5}$  and  $3.8 \times 10^{-5} \text{ cm}^2 \text{V}^{-1} \text{s}^{-1}$  were observed for the layers of PTZ-TROZ, bis-PTZ-TROZ, and tri-PTZ-TROZ, respectively at an electric field of  $6.4 \times 10^5 \text{ Vcm}^{-1}$ . The slight increase of electron mobilities with the increase of the number of PTZ moieties may be apparently explained by the different molecular packing [45]. Considerable effect of the number of PTZ substituents on hole mobilities was observed. At the electric field of  $6.4 \times 10^5 \text{ Vcm}^{-1}$ , hole mobilities increased in the range  $1 \times 10^{-6} < 1.5 \times 10^{-5} < 2.2 \times 10^{-5} \text{ cm}^2 \text{V}^{-1} \text{s}^{-1}$  with an increasing number of phenothiazine units. Among

the studied compounds, the highest hole mobility values were observed for the layers of tri-PTZ-TROZ. They exceeded  $1 \times 10^{-4} \text{ cm}^2 \text{V}^{-1} \text{s}^{-1}$  at electric fields higher than  $1 \times 10^6 \text{ Vcm}^{-1}$  (Fig. 7b).

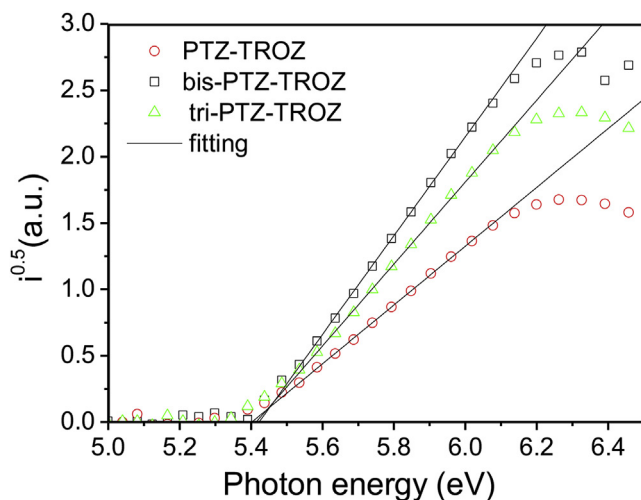
## 2.8. Electroluminescent properties

### 2.8.1. Non-doped fluorescent OLEDs

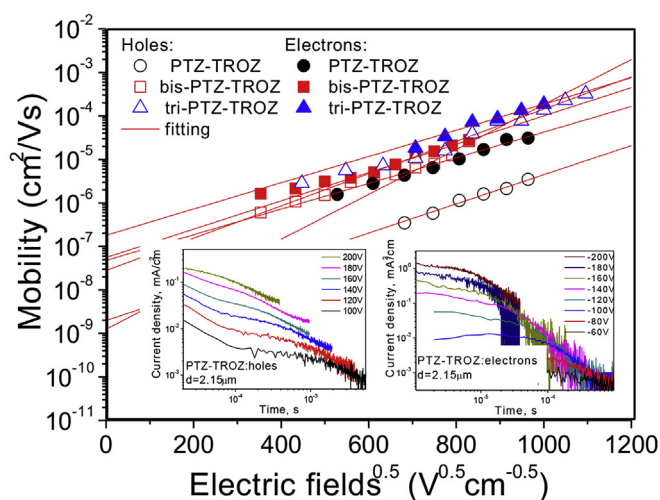
Because of the appropriate charge-injection properties, HOMO/LUMO levels, bipolar charge transport, AIEE and TADF characteristics, the solid films of the compounds were used as non-doped light-emitting layers in OLEDs with the structure ITO/MoO<sub>3</sub>(1 nm)/NPB(30 nm)/TCTA(15 nm)/mCP(5 nm)/light-emitting layer (25 nm)/TSP01(5 nm)/TPBi(30 nm)/LiF(0.5 nm)/Al. Emitting layers of PTZ-TROZ, bis-PTZ-TROZ or tri-PTZ-TROZ were deposited in devices A, B or C, respectively. Energy levels of the functional layers of the fabricated devices are displayed in Fig. 8a. To provide appropriate charge-injection and charge-transport from electrodes to the light-emitting layers, the layers of MoO<sub>3</sub> and LiF were used as the hole and electron injection layers. NPB/TCTA and TPBi were employed as the hole and electron transporting materials, respectively. As a result, a turn-on voltage lower than 4 V was observed for the devices (Fig. 8b). To block excitons within the light-emitting layer [46], the mCP and TSP01 layers were deposited.

The fabricated non-doped devices were characterized by extremely high brightness exceeding  $30000 \text{ cd/m}^2$  (Fig. 8b). At the brightness of  $1000 \text{ cd/m}^2$ , EQEs of devices A, B, and C were found to be 4.92, 4.77, and 4.57%, respectively, i.e., they were only slightly lower than their maximum values (5.4, 4.85, and 5.10%) (Table 4). At the brightness of  $10000 \text{ cd/m}^2$ , the values of EQE were found to be 3.40, 4.38, and 4.00%, respectively. Low roll-off efficiencies of 9, 2, and 10% at the brightness of  $1000 \text{ cd/m}^2$ , and 37, 10, and 22% at the brightness of  $10000 \text{ cd/m}^2$  were observed for devices A, B, and C, respectively (Fig. 8c, Table 4). Because of superior charge transporting properties of bis-PTZ-TROZ and tri-PTZ-TROZ (Fig. 7b), the low-efficiency roll-off was obtained for devices B and C in contrast to that observed for device A.

Yellow to orange emission with the wavelengths of electroluminescence intensity maxima of 555, 570, and 580 nm, corresponding to the Commission Internationale de l'Éclairage (CIE 1931) chromaticity coordinates (x, y) of (0.43, 0.55), (0.47, 0.52), and (0.49, 0.5), were observed for devices A-C (Fig. 8d, Table 4). The slight redshifts of EL spectra of devices B and C in comparison to that of device A were caused by the increasing number of PTZ substituents of the



a)



b)

Fig. 7. Photoelectron emission spectra (a) and charge mobility electric field dependencies (b) for vacuum-deposited films of PTZ-TROZ, bis-PTZ-TROZ, and tri-PTZ-TROZ. Insets: Hole and electron, time-of-flight current transients for the vacuum-deposited film of PTZ-TROZ.

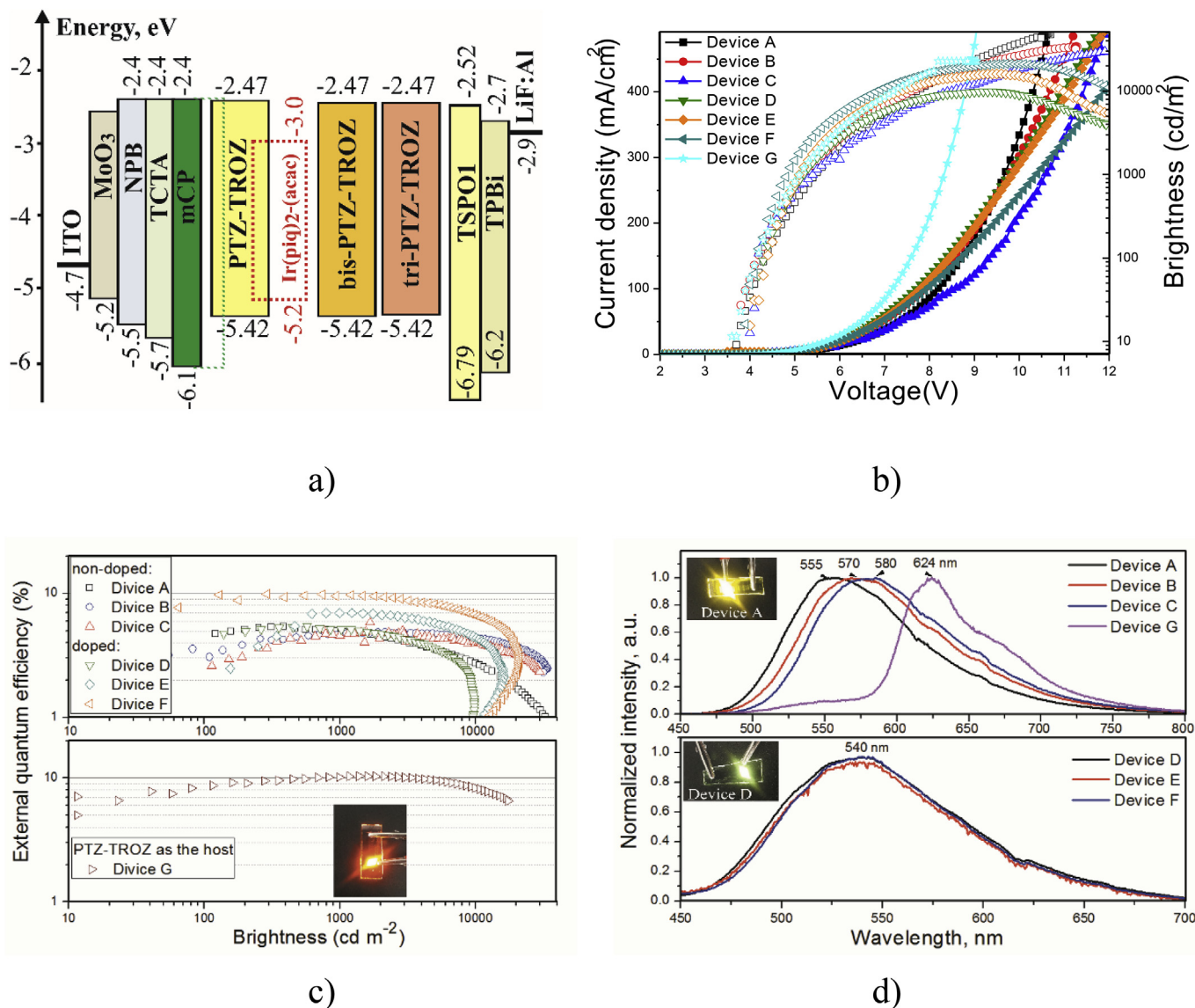


Fig. 8. Equilibrium energy diagram (a), current density–voltage–brightness (b) and EQE–brightness (c) characteristics and EL spectra recorded at 7 V (d) for devices A–G. Insets: photos of PTZ-TROZ-based devices A, D, and G.

Table 4

Output characteristics of non-doped/doped fluorescent and phosphorescent OLEDs.

Device	Light-emitting layer	$V_{on}^a$ V	Max. brightness, cd/m <sup>2</sup>	$EQE_{max}^b$ %	Roll-off, <sup>b</sup> %	$\lambda_{max}^{EL}$ , nm	CIE, <sup>c</sup> (x, y)
Non-doped fluorescent OLEDs using PTZ-TROZ, bis-PTZ-TROZ, or tri-PTZ-TROZ as the AIE/TADF emitters							
A	PTZ-TROZ	3.7	49000	5.4	9/37	555	0.43, 0.55
B	bis-PTZ-TROZ	3.8	33000	4.85	2/10	570	0.47, 0.52
C	tri-PTZ-TROZ	4.0	30000	5.1	10/22	580	0.49, 0.5
Doped fluorescent OLEDs using PTZ-TROZ, bis-PTZ-TROZ, or tri-PTZ-TROZ as the AIE/TADF emitters							
D	PTZ-TROZ:mCP	4.1	9800	5.4	4/74	540	0.33, 0.53
E	bis-PTZ-TROZ:mCP	4.0	16000	7.0	1/37	540	0.32, 0.5
F	tri-PTZ-TROZ:mCP	3.9	21000	9.9	2/34	540	0.33, 0.53
Red phosphorescent OLED using PTZ-TROZ as the AIE/TADF host							
G	PTZ-TROZ:Ir(piq) <sub>2</sub> (acac)	3.6	17000	10.3	1/11	624	0.62, 0.37

<sup>a</sup> Turn-on voltages at 10 cd/m<sup>2</sup>.

<sup>b</sup> Efficiency roll-off efficiency at 1000/10000 cd/m<sup>2</sup> relatively to  $EQE_{max}$ .

<sup>c</sup> CIE for EL spectrum recorded at 7 V.

materials used as the emitters. The stable EL spectra at different applied voltages were in perfect agreement with the PL spectra of vacuum-deposited films of PTZ-TROZ, bis-PTZ-TROZ, or tri-PTZ-TROZ (Fig. S6). Due to the excellent charge-blocking and exciton-blocking properties of the devices, no additional emission was observed in EL spectra of the devices A-C at the different applied voltages (Fig. S5).

Because of the AIE and TADF effects observed for the emitters which were characterized by relatively high PLQYs of 15–37% in solid-state, EQEs of devices A-C exceeded the theoretical limit (5%) of fluorescent OLEDs without outcoupling (Table 4) [47]. The EQE values of devices A-C did not exceed the best EQE values of the published yellow-orange non-doped OLEDs. However the combinations of maximum brightness, EQE and efficiency roll-off values are among the best reported up to now for non-doped OLEDs [48,49].

### 2.8.2. Doped fluorescent OLEDs

In guest-host systems, TADF properties of emitters can be improved by using appropriate host due to the host polarity effect giving high-efficiency RISC [50]. Recently, the enhancement of PLQY for AIEE emitter 4,6-di(9,9-dimethylacridan-10-yl)isophthalonitrile was observed due to its smaller  $\Delta E_{ST}$  in hosted films, which lead to more efficient TADF emission in comparison to that observed for non-doped films [34]. Light-emitting layers containing 5% of each luminophore in mCP were deposited in devices D, E, and F. Higher maximum EQE values of 5.4, 7.0, and 9.9% were observed for devices D, E, and F in comparison to those observed for non-doped devices A, B, and C, correspondingly (Fig. 8c, Table 4). This result can be mainly explained by the higher PLQY values of 64, 67, and 63% for the solid-state molecular mixtures of PTZ-TROZ: mCP, bis-PTZ-TROZ: mCP, and tri-PTZ-TROZ: mCP, respectively. Apparently, TADF efficiency of the studied AIE/TADF luminophores was improved due to the decrease of their  $\Delta E_{ST}$  values in mCP hosted films [51]. At the brightness of 1000 cd/m<sup>2</sup>, devices D, E, and F exhibited the low-efficiency roll-off values of 4, 1, and 2%, respectively, which were similar to their maximum EQE values. However, at the brightness of 10000 cd/m<sup>2</sup>, considerably higher efficiency roll-off values of 74, 37, and 34% were observed (Table 4). In addition, compared with the non-doped devices, the doped devices exhibited the lower maximum brightness. These observations can be explained by dis-balance of hole-electron pairs in the light-emitting layers of the doped devices at high electric fields since the hole-transporting material (mCP) was used as the host [52]. The higher efficiency roll-off values of PTZ-TROZ-based devices A and D can be explained by the different hole and electron mobilities of PTZ-TROZ (Fig. 7b).

Due to the polarity effect of TADF emitters in the guest-host mixtures [53], green electroluminescence was observed for the devices D-F (Fig. 8d). Corresponding to CIE color coordinates (0.33, 0.53), (0.32, 0.5), and (0.33, 0.53), the EL spectra of devices D, E, and F were in good agreement with the PL spectra of the films of the molecular mixtures PTZ-TROZ:mCP, bis-PTZ-TROZ:mCP, and tri-PTZ-TROZ:mCP (Fig. S7).

### 2.8.3. Red phosphorescent OLED

Regarding the bipolar charge transport and appropriate triplet levels, hosting properties of the studied compounds for the red OLEDs were investigated. PTZ-TROZ was used as TADF host in phosphorescent OLEDs (PhOLEDs), which was based on bis(1-phenylisoquinoline)(acetylacetonate)iridium(III) (Ir(piq)<sub>2</sub>(acac)) as an emitter (Device G). The usage of bis-PTZ-TROZ and tri-PTZ-TROZ as TADF hosts for the Ir(piq)<sub>2</sub>(acac) emitter was limited by low deposition rate of these compounds in deep vacuum apparently due to their relatively high molecular weights. Thus, it was not possible to deposit light-emitting layers Ir(piq)<sub>2</sub>(acac):bis-PTZ-TROZ and Ir(piq)<sub>2</sub>(acac):tri-PTZ-TROZ with concentration of 5% of Ir(piq)<sub>2</sub>(acac) in the hosts. In order to provide a comparison of all devices A-G, all functional layers except light-emitting ones were fabricated using the same depositing processes. Despite the fact that a human eye is less sensitive in the red region than in orange or green ones, the brightness of Device G exceeded 10000 cd/m<sup>2</sup>

(Fig. 8b). EL spectra of Device G were mostly related to the emission of Ir(piq)<sub>2</sub>(acac) (Fig. 8d) [54,55]. However, the high-energy band which was related to PTZ-TROZ emission could be recognized. As the host material of PhOLEDs, PTZ-TROZ exhibited great potential. Maximum EQE of 10.3%, low-efficiency roll-offs of 1% at 1000 cd/m<sup>2</sup>, and low-efficiency roll-offs of 11% at 10000 cd/m<sup>2</sup> were observed for device G (Table 4).

## 3. Conclusions

A series of newly designed AIE-TADF materials based on a 1,3,5-triazine acceptor as the core and a phenothiazine donor or a phenoxy donor as the different peripheral units were synthesized and analyzed. These materials were characterized by thermally activated delayed fluorescence and aggregation induced emission enhancement. Photoluminescence quantum yields of up to 37 and 67% were recorded for non-doped and doped solid-state samples. All the synthesized compounds exhibited bipolar charge-transporting properties. The strong effect of phenothiazine substituents on charge-transporting properties of the compounds was demonstrated. The highest charge mobility values were observed for the layers of the compound containing three phenothiazine moieties. They exceeded  $1 \times 10^{-4}$  cm<sup>2</sup>V<sup>-1</sup>s<sup>-1</sup> at electric fields higher than  $1 \times 10^6$  Vcm<sup>-1</sup>. Three types of OLEDs based on the synthesized materials were fabricated. The non-doped yellow device with the compound containing single phenothiazine unit as an emitter gave a maximum external quantum efficiency of 5.4%. OLED with the emissive layer containing 5% solid solution of the compound containing three phenothiazine moieties in 1,3-bis(N-carbazolyl)benzene exhibited maximum external quantum efficiency of 9.9%. Red phosphorescent OLED containing the compound with single phenothiazine moiety as a host showed maximum external quantum efficiency of 10.3% and low efficiency roll-offs of 1% at 1000 cd/m<sup>2</sup>.

## Acknowledgements

This research was funded by the European Regional Development Fund according to the supported activity 'Research Projects Implemented by World-class Researcher Groups' under Measure No. 01.2.2-LMT-K-718. This work was also supported by the Natural Science Foundation of Fujian Province (Grant No. 2016J01233), and Graphene Powder & Composite Research Center of Fujian Province, 2017H2001).

## Appendix A. Supplementary data

Supplementary data to this article can be found online at <https://doi.org/10.1016/j.dyepig.2019.107793>.

## References

- [1] Wong MY, Zysman-Colman E. Purely organic thermally activated delayed fluorescence materials for organic light-emitting diodes. *Adv Mater* 2017;29:1605444.
- [2] Endo A, Sato K, Yoshimura K, et al. Efficient up-conversion of triplet excitons into a singlet state and its application for organic light emitting diodes. *Appl Phys Lett* 2011;98:42.
- [3] Tao Y, Yuan K, Chen T, et al. Thermally activated delayed fluorescence materials towards the breakthrough of organoelectronics. *Adv Mater* 2014;26:7931–58.
- [4] Samanta PK, Kim D, Coropceanu V, et al. Up-conversion intersystem crossing rates in organic emitters for thermally activated delayed fluorescence: impact of the nature of singlet vs triplet excited states. *J Am Chem Soc* 2017;139:4042–51.
- [5] Uoyama H, Goushi K, Shizu K, et al. Highly efficient organic light-emitting diodes from delayed fluorescence. *Nature* 2012;492:234.
- [6] Im Y, Kim M, Cho YJ, et al. Molecular design strategy of organic thermally activated delayed fluorescence emitters. *Chem Mater* 2017;29:1946–63.
- [7] Yang Z, Mao Z, Xie Z, et al. Recent advances in organic thermally activated delayed fluorescence materials. *Chem Soc Rev* 2017;46:915–1016.
- [8] Liu H, Bai Q, Yao L, et al. Highly efficient near ultraviolet organic light-emitting diode based on a meta-linked donor-acceptor molecule. *Chem Sci* 2015;6:3797–804.
- [9] Liu Y, Li C, Ren Z, et al. All-organic thermally activated delayed fluorescence materials for organic light-emitting diodes. *Nat Rev Mater* 2018;3:18020.

- [10] Tanaka H, Shizu K, Miyazaki H, et al. Efficient green thermally activated delayed fluorescence (TADF) from a phenoxazine-triphenyltriazine (PXZ-TRZ) derivative. *Chem Commun* 2012;48:11392-4.
- [11] Hirata S, Sakai Y, Masui K, et al. Highly efficient blue electroluminescence based on thermally activated delayed fluorescence. *Nat Mater* 2015;14:330-6.
- [12] Wang ZH, Li YC, Cai XY, et al. Structure-performance investigation of thioxanthone derivatives for developing color tunable highly efficient thermally activated delayed fluorescence emitters. *ACS Appl Mater Interfaces* 2016;8:8627-36.
- [13] Lee JY, Shizu K, Tanaka H, et al. Oxadiazole- and triazole-based highly-efficient thermally activated delayed fluorescence emitters for organic light-emitting diodes. *J Mater Chem C* 2013;1:4599-604.
- [14] Santos PL, Ward JS, Data P, et al. Engineering the singlet-triplet energy splitting in a TADF molecule. *J Mater Chem C* 2016;4:3815-24.
- [15] Zhang Q, Li B, Huang S, et al. Efficient blue organic light-emitting diodes employing thermally activated delayed fluorescence. *Nat Photonics* 2014;8:326.
- [16] Gudeika D, Grazulevicius JV, Volyniuk D, et al. Effect of ethynyl linkages on the properties of the derivatives of triphenylamine and 1, 8-naphthalimide. *J Phys Chem C* 2015;119:28335-46.
- [17] Luo J, Xie Z, Lam JWY, et al. Aggregation-induced emission of 1-methyl-1,2,3,4,5-pentaphenylsilole. *Chem Commun* 2001;18:1740-1.
- [18] Jana D, Ghorai BK. Synthesis and aggregation-induced emission properties of tetraphenylethylene-based oligomers containing triphenylethylene moiety. *Tetrahedron Lett* 2012;53:6838-42.
- [19] Gong Y, Tan Y, Liu J, et al. Twisted D-pi-A solid emitters: efficient emission and high contrast mechanochromism. *Chem Commun* 2013;49(38):4009-11.
- [20] Hong Y, Lam JW, Tang BZ. Aggregation-induced emission: phenomenon, mechanism and applications. *Chem Commun* 2009;29:4332-53.
- [21] Fan ZX, Zhao QH, Wang S, et al. Polyurethane foam functionalized with an AIEactive polymer using an ultrasonication-assisted method: preparation and application for the detection of explosives. *RSC Adv* 2016;6:26950-3.
- [22] Chu ZW, Fan ZX, Zhang X, et al. A comparison of ACQ, AIE and AEE-based polymers loaded on polyurethane foams as sensors for explosives detection. *Sensors* 2018;18:1565.
- [23] Xu S, Liu T, Mu Y, et al. An organic molecule with asymmetric structure exhibiting aggregation-induced emission, delayed fluorescence, and mechanoluminescence. *Angew Chem Int Ed* 2015;54:874-8.
- [24] Zhao YD, Wang WG, Gui C, et al. Thermally activated delayed fluorescence material with aggregation-induced emission properties for highly efficient organic light-emitting diodes. *J Mater Chem C* 2018;6:2873-81.
- [25] Tanaka H, Shizu K, Miyazaki H, et al. Efficient green thermally activated delayed fluorescence (TADF) from a phenoxazine-triphenyltriazine (PXZ-TRZ) derivative. *Chem Comm* 2012;48:11392-4.
- [26] Yao L, Pan Y, Tang X, et al. Tailoring excited-state properties and electroluminescence performance of donor-acceptor molecules through tuning the energy level of the charge-transfer state. *J Phys Chem C* 2015;119:17800-8.
- [27] Marghad I, Clochard MC, Ollier N, et al. Thermally activated delayed fluorescence evidence in non-bonding transition electron donor-acceptor molecules. *PROC SPIE XIX* 2015;9566:956629.
- [28] Lu T, Chen F. Multiwfn: a multifunctional wavefunction analyzer. *J Comput Chem* 2012;33:580-92.
- [29] Lu T. Multiwfn program, Version 3.6.
- [30] Tao SL, Peng ZK, Zhang XH, et al. Highly efficient non-doped blue organic light-emitting diodes based on fluorene derivatives with high thermal stability. *Adv Funct Mater* 2005;15:1716-21.
- [31] Hung YC, Jiang JC, Chao CY, et al. Theoretical study on the correlation between band gap, bandwidth, and oscillator strength in fluorene-based Donor-acceptor conjugated copolymers. *J Phys Chem B* 2009;113:8268-77.
- [32] Vigante B, Leitonas K, Volyniuk D, et al. Synthesis of linear and V-shaped carbazolyl-substituted pyridine-3,5-dicarbonitriles exhibiting efficient bipolar charge transport and E-type fluorescence. *Chemistry-Eur J* 2018;25:3325-36.
- [33] Chen Y, Lam JWY, Kwok RTK, et al. Aggregation-induced emission: fundamental understanding and future developments. *Mater Horizons* 2019;6:428-33.
- [34] Skuodis E, Bezikonny O, Tomkeviciene A, et al. Aggregation, thermal annealing, and hosting effects on performances of an acridan-based TADF emitter. *Org Electron* 2018;63:29-40.
- [35] Kukhta NA, Filho DAS, Volyniuk D, et al. Can fluorenone-based compounds emit in the blue region? Impact of the conjugation length and the ground-state aggregation. *Chem Mater* 2017;29:1695-707.
- [36] Han C, Zhang Z, Ding D, et al. Dipole-dipole interaction management for efficient blue thermally activated delayed fluorescence diodes. *Chem* 2018;4:2154-67.
- [37] Zhang Q, Li B, Huang S, et al. Efficient blue organic light-emitting diodes employing thermally activated delayed fluorescence. *Nat Photonics* 2014;8:326.
- [38] Dong Y, Lam JWY, Qin A, et al. Aggregation-induced emissions of tetraphenylethene derivatives and their utilities as chemical vapor sensors and in organic light-emitting diodes. *Appl Phys Lett* 2007;91:011111.
- [39] Gao Y, Qu Y, Jiang T, et al. Alkyl-triphenylamine end-capped triazines with AIE and large two-photon absorption cross-sections for bioimaging. *J Mater Chem C* 2014;2:6353-61.
- [40] Hong Y, Lam JWY, Tang BZ. Aggregation-induced emission. *Chem Soc Rev* 2011;40:5361-88.
- [41] Mei J, Leung NLC, Kwok RTK, et al. Aggregation-induced emission: together we shine, united we soar. *Chem Rev* 2015;115:11718-940.
- [42] Mimaite V, Grazulevicius JV, Laurinaviciute R, et al. Can hydrogen bonds improve the hole-mobility in amorphous organic semiconductors? Experimental and theoretical insights. *J Mater Chem C* 2015;3:11660-74.
- [43] Kukhta NA, Simokaitiene J, Volyniuk D, et al. Effect of linking topology on the properties of star-shaped derivatives of triazine and fluorene. *Synthetic Met* 2014;195:266-75.
- [44] Arkhipov VI, Fishchuk II, Kadashchuk A, et al. Charge transport in disordered organic semiconductors. *Photophysics of Molecular Materials: from single molecules to single crystals*. 2005. p. 261-366.
- [45] Grybauskaitė-Kaminskiene G, Volyniuk D, Mimaite V, et al. Aggregation-enhanced emission and thermally activated delayed fluorescence of derivatives of 9-phenyl-9H-carbazole: effects of methoxy and tert-butyl substituents. *Chem Eur J* 2018;24:9581-91.
- [46] Sallenave X, Bucinskas A, Salman S, et al. Sensitivity of redox and optical properties of electroactive carbazole derivatives to the molecular architecture and methoxy substitutions. *J Phys Chem C* 2018;122:10138-52.
- [47] Tsutsui T. Progress in electroluminescent devices using molecular thin films. *MRS Bull* 1997;22:39-45.
- [48] Guo J, Zhao Z, Tang BZ. Purely organic materials with aggregation-induced delayed fluorescence for efficient nondoped OLEDs. *Adv Opt Mater* 2018;1800264.
- [49] Rizzo F, Cucinotta F. Recent developments in AIEgens for non-doped and TADF OLEDs. *Isr J Chem* 2018;58:874-88.
- [50] Etherington MK, Gibson J, Higginbotham HF, et al. Revealing the spin-vibronic coupling mechanism of thermally activated delayed fluorescence. *Nat Commun* 2016;7:13680.
- [51] Tomkeviciene A, Sutaite J, Volyniuk D, et al. Aggregation-induced emission enhancement in charge-transporting derivatives of carbazole and tetra (tri) phenylethylene. *Dyes Pigments* 2017;140:363-74.
- [52] Wu MF, Yeh SJ, Chen CT, et al. The quest for high-performance host materials for electrophosphorescent blue dopants. *Adv Funct Mater* 2007;17:1887-95.
- [53] Méhes G, Goushi K, Potscavage Jr. WJ, et al. Influence of host matrix on thermally-activated delayed fluorescence: effects on emission lifetime, photoluminescence quantum yield, and device performance. *Org Electron* 2014;15:2027-37.
- [54] Su YJ, Huang HL, Li CL, et al. Highly efficient red electrophosphorescent devices based on iridium isoquinoline complexes: remarkable external quantum efficiency over a wide range of current. *Adv Mater* 2003;15:884-8.
- [55] Bezikonny O, Gudeika D, Volyniuk D, et al. Pyrenyl substituted 1, 8-naphthalimide as a new material for weak efficiency-roll-off red OLEDs: a theoretical and experimental study. *New J Chem* 2018;42:12492-502.